JOURNAL OF GUIDANCE, CONTROL, AND DYNAMICS
Vol. 24, No. 4, July–August 2001

# Selective Modal Control Theory for Piezolaminated Anisotropic Shells

Scott E. Miller*
*Orbital Sciences Corporation, Beltsville, Maryland 20705*
and
Yaakov Oshman† and Haim Abramovich‡
*Technion—Israel Institute of Technology, 32000 Haifa, Israel*

**A general selective modal control design methodology is presented for piezolaminated anisotropic shell systems, which uses selective modal transducers recently developed by the authors for piezo-shells in order to realize any number of possible modal control strategies. A selective modal control design procedure, which defines a step-by-step framework through which structural and control subdesign processes are effectively integrated, is specified. Several conditions that sufficiently ensure asymptotic stability are derived and then discussed in the context of deriving selective modal control methods, which are stability-robust to modeling and implementation errors. Several design examples are given. A numerical example is then presented in which a stability-robust optimal selective modal control design is developed for a cantilevered anisotropic cylindrical shell panel. Maintaining a linear feedback law, a selective modal transducer is employed, whose design parameters were chosen so as to optimize the system response to a given initial excitation. Frequency and transient response analyses demonstrate a dramatic enhancement in system performance and are shown to accurately concur with theoretical predictions.**

## I. Introduction

WITHIN the past decade several vibration control techniques have been developed for simple beam and plate systems, which use distributed piezoelectric transducers formed from polyvinylidine fluoride (PVDF). PVDF actuators whose spatially varying piezoelectric field properties were exploited to provide for the simultaneous control of all modes or special modal subsets in cantilevered and simply supported beams have been designed.[1,2] Miller and Hubbard developed a reciprocal sensor theory and subsequently incorporated PVDF sensors and actuators into multicomponent systems in which each component itself was a smart structural member.[3] Burke and Hubbard[4] developed a formulation for the control of thin elastic (Kirchhoff–Love) isotropic plates subject to most combinations of free, clamped, or pinned boundary conditions, in which the active elements were spatially varying biaxially polarized piezoelectric transducer layers. Lee[5] generalized the classical laminate plate theory to include the effect of laminated piezoelectric layers and thus to provide a theoretical framework for the distributed transduction of bending, torsion, shearing, shrinking, and stretching in flexible anisotropic plates. Miller et al.[6] subsequently employed Lyapunov's second method to derive a general active vibration suppression control design methodology for anisotropic laminated piezoelectric plates.

The aforementioned vibration control strategies share several common limitations. Although all of these methods reduce the vibration control task to a selection of individual piezolamina field functions, none offers a general method for determining those field functions so as to ensure active vibration suppression. A poor choice in piezo-field functions, although guaranteed not to destabilize the structure through the active addition of vibrational energy, can extract little or no vibrational energy from the system. Furthermore, often the designer is concerned with suppressing vibrations in only a certain modal subset. The generalized function approach to choosing spatial field functions,[2,4] although adequate in certain scenarios for guaranteeing some measure of active energy extraction from all modes, generally will not be able to provide a means to selectively target a specific modal subset. Finally, most methodologies just mentioned have been exclusive to isotropic systems and are thus incompatible for use with orthotropic and anisotropic aeroelastic structures commonly encountered. Ultimately these limitations would be best answered through the development of a selective modal control (SMC) methodology in which the designer optimally uses embedded piezolaminas to most effectively realize any admissible performance objective. The authors recently developed such a methodology for anisotropic plates[7] and validated their results through both numerical and experimental analyses.[8]

This paper extends the SMC theory to piezolaminated anisotropic shell systems and in particular those shell systems whose geometries are deformable onto a plane. A broad class of stability robust SMC approaches is defined through the identification of sufficient conditions that ensure global asymptotic stability without requiring perfect knowledge of design parameters, structural constants, or modal behavior. Specific SMC design examples are given, and the design approach is illustrated via a numerical example involving a piezolaminated anisotropic cylindrical panel.

## II. System Description

### A. Geometry

Figure 1 provides a geometric definition of the composite shell structure under consideration. There exist exactly $N$ laminated layers, all of which are considered to be piezoelectrically active: piezoelectric constants relative to the nonpiezoelectric substructure are set to zero. Material properties within each lamina are assumed continuous. The electromechanical transduction effect of each lamina can vary spatially. An orthogonal curvilinear coordinate frame is defined by the unit vectors $\hat{\alpha}_1$, $\hat{\alpha}_2$, and $\hat{\alpha}_3$. Piezolaminas sublayers are assumed to be transversely anisotropic, that is, monoclinic relative to the $\hat{\alpha}_3$ axis. The reference surface of the shell is located on the $\alpha_3 = (\alpha_3)_0$ plane. The reference plane itself can be arbitrarily located, although it is typically assigned to the structural midplane. In orthotropic and isotropic structures, however, the reference plane is designated as the neutral plane. Defining the distance in the $\hat{\alpha}_3$ direction between any arbitrary point and the reference plane as $z$, any arbitrary point $(\alpha_1, \alpha_2, \alpha_3)$ can be equivalently expressed as $[\alpha_1, \alpha_2, (\alpha_3)_0 + z]$. The infinitesimal distance $ds$ between two

Received 19 January 1999; revision received 15 June 2000; accepted for publication 4 August 2000. 

*Scientist, Special Payloads, Mail Stop GB-3, 5010 Herzel Place. Member AIAA.
†Associate Professor, Department of Aerospace Engineering. Associate Fellow AIAA.
‡Senior Lecturer, Department of Aerospace Engineering. Senior Member AIAA.

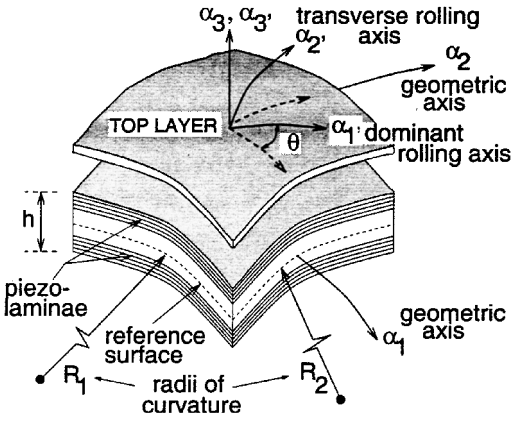


**Fig. 1 Geometry of general piezolaminated shell system.**

arbitrary points $(\alpha_1, \alpha_2, \alpha_3)$ and $(\alpha_1 + d\alpha_1, \alpha_2 + d\alpha_2, \alpha_3 + d\alpha_3)$ of a shell element in the curvilinear frame is given as[9]

$$ds^2 = L_1^2(d\alpha_1)^2 + L_2^2(d\alpha_2)^2 + d\alpha_3^2 \tag{1}$$

where the Lamé coefficients $L_1$ and $L_2$ are defined as

$$L_1 \triangleq A_1(1 + z/R_1), \qquad L_2 \triangleq A_2(1 + z/R_2) \tag{2}$$

and $A_1$ and $A_2$ are the Lamé parameters.[10] $R_1$ and $R_2$ are the radii of curvature corresponding to the $\hat{\alpha}_1$ and $\hat{\alpha}_2$ directions, respectively. Lamé parameters and radii of curvature for several common structural geometries can be found in the literature.[9] The discussion to follow is limited to zero-Gaussian curvature shells, that is, shell geometries defined such that $1/R_1R_2 = 0$, which include all geometries that are developable onto a plane.

The $\hat{\alpha}_3$ locations of the surfaces of each individual lamina are defined such that the bottom layer of the composite shell is assigned the index $k = 1$ and the indices increase unitarily. The distance from the reference surface to the lower, upper, and middle surfaces of any given lamina are respectively defined as $z_{k-1}$, $z_k$, and $z_k^0$. The thickness of any given lamina is defined as $h^k$. The composite reference surface is displaced at some distance $(\alpha_3)_0$ from the origin of the coordinate frame. The composite thickness is defined as $h$. The upper and lower surfaces of the composite are respectively located at heights $z_N$ and $z_0$.

### B. Equations of Motion

Using either first-order shear deformation theory (FOSDT) or classical Kirchhoff–Love approximations, the equations of motion of the general system described in Fig. 1 can be derived and expressed in the explicit form[11]

$$\boldsymbol{x}_{tt} + \mathcal{C}\boldsymbol{x}_t + \mathcal{K}\boldsymbol{x} = \frac{1}{\rho h A_1 A_2}\mathcal{D}^T\left(\sum_{k=1}^{N} \boldsymbol{e}_0^k \Lambda^k V^k\right) \tag{3}$$

$$q^k(t) = \iint_A \frac{1}{A_1 A_2}(\mathcal{E}\boldsymbol{x})^T \boldsymbol{e}_0^k \Lambda^k \, \mathrm{d}A + C^k V^k \tag{4}$$

where the subscript $t$ refers to partial differentiation with respect to time and $A$ is the surface area of the shell. Boundary conditions are stated in Ref. 11. Equation (3) is the mechanical displacement equation of motion, while Eq. (4) is the (definite) integral form of the electrostatic charge displacement equation for this class of materials. Equations (3) and (4) can be respectively considered as the governing actuator and sensor equations, where $\boldsymbol{x}$ is a vector of mechanical displacements, $q^k(t)$ is the electrostatic charge displacement relative to the $k$th sublaminate, and $V^k(t)$ is the voltage applied across the $k$th sublaminate. The capacitance of the $k$th sublaminate is given as $C^k$. The composite mass density is given as $\rho$, while $\mathcal{D}$ and $\mathcal{E}$ are ordinary linear differential operators defined in Ref. 11. The (mass-normalized) stiffness operator $\mathcal{K}$ is a fourth-order positive semidefinite and self-adjoint differential operator[11] and is defined as

$$\mathcal{K} \triangleq \frac{1}{\rho h A_1 A_2}\mathcal{D}^T \frac{1}{A_1 A_2}\begin{bmatrix} \boldsymbol{A} & \boldsymbol{B} \\ \boldsymbol{B} & \boldsymbol{D} \end{bmatrix}\mathcal{E} \tag{5}$$

where $\boldsymbol{A}$, $\boldsymbol{B}$, and $\boldsymbol{D}$ are matrices of constitutive mechanical constants that characterize the mechanical stress-strain behavior of the composite system. The damping operator $\mathcal{C}$ can be any operator that commutes with $\mathcal{K}$ and satisfies

$$\langle \phi_i, \mathcal{C}\phi_j \rangle = c_j(t)\delta_{ij}, \qquad \begin{matrix} c_j(t) > 0 \ \forall \ t > 0 \\ c_j(0) = 0 \end{matrix} \tag{6}$$

where $c_j(t)$ is piecewise differentiable, $\phi_j$ is the $j$th eigenvector of $\mathcal{K}$ and $\delta_{ij}$ is the Kronecker delta function. The electromechanical field strength of each piezolamina is described mathemetically via the product $\boldsymbol{e}_0^k\Lambda^k$, where $\Lambda^k = \Lambda^k(\alpha_1, \alpha_2)$ is a dimensionless and spatially varying piezoelectric field distribution function and

$$\boldsymbol{e}_0^k \triangleq \left[\left(e_{31}^k\right)_0 \quad \left(e_{32}^k\right)_0 \quad \left(e_{36}^k\right)_0 \quad z_k^0\left(e_{31}^k\right)_0 \quad z_k^0\left(e_{32}^k\right)_0 \quad z_k^0\left(e_{36}^k\right)_0\right]^T \tag{7}$$

The piezoconstants $(e_{31}^k)_0$, $(e_{32}^k)_0$, and $(e_{36}^k)_0$ are defined relative to the point of maximum electromechanical transduction so that $\Lambda^k$ is normalized, that is, the maximum value of $\Lambda^k$ is unity.

Equation (4) can be rendered into more advantageous forms by recalling that the measured current is by definition the time derivative of the developed charge and that the voltage measured across the electrode surfaces is found by dividing the developed charge by the film capacitance. In practice an output measurement, which is directly related to mechanically induced strain, is desired. Thus the most useful sensor current or voltage relationships are found by manipulating Eq. (4) such that

$$i_s^k(t) = i_m^k(t) - C_p^k\frac{\mathrm{d}V^k}{\mathrm{d}t} = \iint_A \frac{1}{A_1 A_2}(\mathcal{E}\boldsymbol{x}_t)^T \boldsymbol{e}_0^k \Lambda^k \, \mathrm{d}A \tag{8}$$

$$V_s^k(t) = V_m^k(t) - V^k(t) = \frac{1}{C_p^k}\iint_A \frac{1}{A_1 A_2}(\mathcal{E}\boldsymbol{x})^T \boldsymbol{e}_0^k \Lambda^k \, \mathrm{d}A \tag{9}$$

where $i_m^k(t)$ and $V_m^k(t)$ are the $k$th lamina current and voltage direct measurements. The consequence of Eqs. (8) and (9) is that the same piezoelectric layer can be used simultaneously as both a sensor and as an actuator through the use of differential circuitry and electronics.[12]

## III. Selective Modal Transducer Theory

### A. Description

In Ref. 11 a selective modal transducer (SMT) theory was presented that allows for the selective excitation and detection of each and every mode of an anisotropic piezolaminated thin shell. SMTs are critical to the development of a SMC methodology.

The following set of SMT construct conditions are imposed:

*Condition C1:* Exactly $n$ transducer layers are located strictly above the reference surface and exactly $n$ transducers are located strictly below the reference surface ($N = 2n$).

*Condition C2:* There are at least six piezoelectrically active layers ($2n \geq 6$).

*Condition C3:* For each layer above the reference surface, there exists a layer below the reference surface such that $\{z^k = -z^{k+n}\}_{k=1}^n$.

*Condition C4:* Layers located at heights $z^k$ and $z^{k+n}$ both are associated with the identical piezo-property vector $\boldsymbol{e}_0^k$.

*Condition C5:* The piezo-property vectors $\{\boldsymbol{e}_0^k\}_{k=1}^n$ associated with at least three layers above and likewise below the reference surface are different.

Adhering to the preceding conditions leads to the following lemma, proven in Ref. 11.

*Lemma 1:* Let $\boldsymbol{R} < \Re^{6,6}$ be the matrix defined as

$$\boldsymbol{R} \triangleq \sum_{k=1}^{N} \boldsymbol{e}_0^k \left(\boldsymbol{e}_0^k\right)^T \tag{10}$$

Then, if C1–C5 hold, $\boldsymbol{R}$ is invertible.

Lemma 1 is central to SMT formulations for both FOSDT and classical Kirchhoff–Love system descriptions. Although the FOSDT-based SMT formulation yields the same central result, for simplicity the SMT central theorem that follows is stated for a system whose equations of motion are governed by Kirchhoff–Love assumptions. The following theorem was proven in Ref. 11.

*Theorem 1:* Consider an anisotropic (Kirchhoff–Love) thin shell containing $N$ piezolaminas whose equations of motion are given by Eq. (3). Assume that each lamina is to function as a self-sensing actuator such that the sensed measurement of the $k$th layer is given by Eq. (8). Let the measured state $i_s(t)$ be formed from the weighted sum of the sensed currents of each individual lamina such that

$$i_s(t) = \sum_{k=1}^{N} g_0^k i_s^k(t)$$

Let the time-bound control input $V^k(t)$ of each piezolamina be proportional to an identical time-dependent control function $V_a(t)$, such that $V^k(t) = g_0^k V_a(t)$. Assume that C1-C5 are satisfied. If the piezoelectric field distribution functions of each active layer are given by

$$\Lambda^k = \frac{1}{g_0^k}\left(\boldsymbol{e}_0^k\right)^T \boldsymbol{R}^{-1} \frac{1}{A_1 A_2} \begin{bmatrix} \boldsymbol{A} & \boldsymbol{B} \\ \boldsymbol{B} & \boldsymbol{D} \end{bmatrix} \mathcal{E}\bar{\phi} \tag{11}$$

where the weighted modal sum

$$\bar{\phi} \triangleq \sum_{j=1}^{\infty} \alpha_j \phi_j$$

and the scaling factor $g_0$ is defined as

$$g_0^k = \max_{(\alpha_1,\alpha_2)\in A} \left| \left(\boldsymbol{e}_0^k\right)^T \boldsymbol{R}^{-1} \frac{1}{A_1 A_2} \begin{bmatrix} \boldsymbol{A} & \boldsymbol{B} \\ \boldsymbol{B} & \boldsymbol{D} \end{bmatrix} \mathcal{E}\bar{\phi} \right| \tag{12}$$

then the measured state is reduced to the form

$$i_s(t) = \rho h \sum_{j=1}^{\infty} \alpha_j \lambda_j \dot{q}_j(t) \tag{13}$$

and the mechanical equation of motion [Eq. (3)] is reduced to the form

$$\ddot{q}_j + c_j \dot{q}_j + \lambda_j q_j = \alpha_j \lambda_j V_a(t) \tag{14}$$

for all integers $j > 0$, where $\alpha_j$, $\lambda_j$, and $\dot{q}_j$ are respectively the modal participation factor, eigenvalue, and generalized modal velocity associated with the $j$th eigenfunction.

### B. Discussion

*1. Controllability and Observability*

The conditions stated in Theorem 1 are sufficient to ensure complete controllability and observability. There may exist simpler conditions that can guarantee the same.

*2. Self-Sensing Actuation*

For the sake of generality, Theorem 1 assumes that each piezosublaminate functions as a self-sensing actuator, yielding an SMT that functions as a self-sensing modal actuator (SSMA). Each layer can also assume dedicated actuator or sensing functions so as to yield an SMT that functions as a dedicated selective modal actuator (SMA) or a selective modal sensor (SMS).[11]

*3. Required Number of Layers*

For an anisotropic structure no more than six piezolayers are required to guarantee complete controllability and observability of every structural mode.[11] Any advantage of employing more than six layers needs to be traded against fabrication complexity, increased structural stiffness, etc. For orthotropic structures no more than three layers are required. A single layer is sufficient to provide complete controllability and observability of an isotropic structure.[11]

*4. Layer Placement*

The piezoelectric field functions and gains [Eqs. (11) and (12)] are implicitly related to $z^k$ so that SMT performance is insensitive to the distance from the neutral plane. Electrical continuity, bonding, and other fabrication concerns are critical to the design process. Many of these issues were investigated in a recent experimental demonstration of the SMT design on an orthotropic plate.[8]

## IV. Selective Modal Control

SMTs can be used to implement a number of modal control strategies for composite shells in which both the SMT design and control law are chosen so as to optimize or else prespecify the dynamic response of a targeted modal subset. These SMC strategies can be designed so as to guarantee asymptotic stability regardless of errors that occur in the design process. Moreover, the freedom to arbitrarily determine SMT behavior as part of the design process typically leads to enhanced system performance and reduced burden on the control law itself.

### A. General Definition

The system description is now further generalized to include the possibility of multiple SMTs. Multiple SMTs, although not required for controllability, are considered in order to provide more options for realizing a desired design objective. The independent modal control (IMC) approach,[13] for example, would require as many SMTs as targeted modes. Although each mode could be controlled independently, an alternative control strategy using a single SMT to control multiple modes can be theoretically less optimal but drastically simpler to fabricate and implement. On the other hand, an IMC implementation could be the best approach for controlling a few modes of an isotropic structure because isotropic structures require only a single piezolayer per SMT.

Theorem 1 states that if certain conditions (C1–C5) regarding the location, orientation, number, and electromechanical transduction of piezosublaminas are obeyed then the SMT design process allows for the equations of motion of an anisotropic composite shell to be reduced to the form of Eqs. (13) and (14). Assuming that each SMT requires exactly $N$ piezo-sublaminas and assuming the existence of exactly $p$ dedicated SMAs and $q$ dedicated SMSs, the general mechanical equation of motion of the form

$$\boldsymbol{x}_{tt} + \mathcal{C}\boldsymbol{x}_t + \mathcal{K}\boldsymbol{x} = \frac{1}{\rho h A_1 A_2} \mathcal{D}^T \left( \sum_{k=1}^{p\cdot N} \boldsymbol{e}_0^k \Lambda^k V^k \right) \tag{15}$$

can be reduced via Theorem 1 to the expression

$$\ddot{q}_m + c_m \dot{q}_m + \lambda_m q_m = \sum_{l=1}^{p} \alpha_m^l \lambda_m V_a^l(t) \tag{16}$$

while the $q$ SMS output equations become

$$i_s^n(t) = \rho h \sum_{j=1}^{\infty} \beta_j^n \lambda_j \dot{q}_j(t), \qquad n \in [1, 2, \ldots, q] \tag{17}$$

The driving voltage of the $l$th SMA ($l \in [1, \ldots, p]$) is referred to as $V_a^l(t)$ and the measured current of the $n$th SMS ($n \in [1, \ldots, q]$) as $i_s^n(t)$. If the $l$th SMA is self-sensing (i.e., an SSMA), then for some $n \in [1, \ldots, q]$, $l = n$ and $\beta_j^n = \alpha_j^l$ for all $j$. The $m$th mode is controllable only if at least one $\alpha_m^l \neq 0$ for some $l \in [1, \ldots, p]$ and observable only if at least one $\beta_m^l \neq 0$ for some $l \in [1, \ldots, q]$. Let $R$ be an $r$-dimensional subset of modes targeted for active control. Because $\alpha_m^l, \beta_m^n = 0 \ \forall \ m \notin R$, then from Eqs. (16) and (17) each excluded mode is completely decoupled from all other modes and hence will not lead to spillover in any active control strategy based

solely on the targeted subset. Considering only the $r$ modes in $R$, Eqs. (16) and (17) can be constructed in the form

$$\frac{\mathrm{d}}{\mathrm{d}t}\begin{bmatrix} q_1 \\ \vdots \\ qr \\ \dot{q}_1 \\ \vdots \\ \dot{q}_r \end{bmatrix} = \left[\begin{array}{ccc|ccc} 0 & & & 1 & & \\ & \ddots & & & \ddots & \\ & & 0 & & & 1 \\ \hline -\lambda_1 & & & -c_1 & & \\ & \ddots & & & \ddots & \\ & & -\lambda_r & & & -c_r \end{array}\right]\begin{bmatrix} q_1 \\ \vdots \\ qr \\ \dot{q}_1 \\ \vdots \\ \dot{q}_r \end{bmatrix} + \left[\begin{array}{ccc} 0 & & \\ & \ddots & \\ & & 0 \\ \hline \alpha_1^1\lambda_1 & \cdots & \alpha_1^p\lambda_1 \\ \vdots & \ddots & \vdots \\ \alpha_r^1\lambda_r & \cdots & \alpha_r^p\lambda_r \end{array}\right]\begin{bmatrix} V_a^1 \\ \vdots \\ V_a^p \end{bmatrix}$$

$$\begin{bmatrix} i_s^1/\rho h \\ \vdots \\ i_s^q/\rho h \end{bmatrix} = \left[\begin{array}{ccc|ccc} 0 & & & \beta_1^1\lambda_1 & \cdots & \beta_r^1\lambda_r \\ & \ddots & & \vdots & \ddots & \vdots \\ & & 0 & \beta_1^q\lambda_1 & \cdots & \beta_r^q\lambda_r \end{array}\right]\begin{bmatrix} q_1 \\ \vdots \\ qr \\ \dot{q}_1 \\ \vdots \\ \dot{q}_r \end{bmatrix} \tag{18}$$

or in abbreviated notation

$$\dot{\boldsymbol{x}}_a = \boldsymbol{A}\boldsymbol{x}_a + \begin{bmatrix} 0 \\ \boldsymbol{\alpha} \end{bmatrix}\boldsymbol{V}, \qquad \boldsymbol{i} = [0 \quad \boldsymbol{\beta}^T]\boldsymbol{x}_a \tag{19}$$

where $\boldsymbol{x}_a^T \triangleq [\boldsymbol{q}_a^T \;\; \dot{\boldsymbol{q}}_a^T]^T$ and the matrix definitions are obvious. For convenience the output vector $\boldsymbol{i}$ contains the $q$ SMS current outputs normalized relative to $\rho h$. The matrices $\boldsymbol{\alpha} \in \Re^{r,p}$ and $\boldsymbol{\beta} \in \Re^{r,q}$ are defined such that if the $k$th SMA is self-sensing then the $k$th columns of $\boldsymbol{\alpha}$ and $\boldsymbol{\beta}$ are identical. If all SMAs are self-sensing (and no dedicated SMSs exist), $\boldsymbol{\alpha} = \boldsymbol{\beta}$.

SMC is realized when the matrices $\boldsymbol{\alpha}$, $\boldsymbol{\beta}$, and a control law of the general form $\boldsymbol{V} = \boldsymbol{V}(\boldsymbol{i})$ are established so as to best satisfy a given performance objective. Design parameters can be chosen either directly or else through the optimization of a general performance index of the form $\mathcal{J} = \mathcal{J}(\boldsymbol{x}_a, \boldsymbol{\alpha}, \boldsymbol{\beta})$. In general terms, an SMC design evolves through a step-by-step process: 1) a composite shell structural design is determined so as to satisfy any mechanical requirements (mass, stiffness, fabrication complexity, etc.); 2) the structure is modeled; 3) a suitable performance objective is established and then optimized subject to Eq. (19) to determine a suitable control law and set of modal participation factors (MPFs); and 4) the design is assessed, and, if no further reiteration is required, the piezo-field functions ($\Lambda^k$) for each piezolamina are determined via Eq. (11). The design is then implemented physically. Some of these steps are now briefly considered.

### 1. *Structural Design*

The process of satisfying structural requirements will necessarily dictate the number of piezolaminas to be incorporated and hence the number of available SMTs. The structure must be designed such that all SMT construct conditions are satisfied (conditions C1–C5). At least six laminas per anisotropic shell SMT are required, whereas orthotropic and isotropic shells require three or fewer layers. From a control standpoint the advantage of multiple SMTs may be small, as many control design objectives are likely to be sufficiently attainable even via a single SSMA.

### 2. *Performance Objective*

Having obtained a satisfactory representation of Eq. (19), performance objectives must be determined, which will dictate the dynamic character of the actively controlled shell as well as the stability robustness of the system to errors that will inevitably occur during the modeling and implementation phases. The consequence of such errors is that the field distribution functions ($\Lambda^k$), which are ultimately implemented, will lead to an imperfect realization of the MPFs (residing in $\boldsymbol{\alpha}$ and $\boldsymbol{\beta}$) specified as the outcome of the design process. Stability robustness is therefore assessed in terms of the sensitivity of a given design to perturbations in $\boldsymbol{\alpha}$ and $\boldsymbol{\beta}$. In the sections that immediately follow, criteria are determined to assess the stability robustness of a given design, and a number of representative performance objectives are discussed.

## B. Stability Robust SMC

In this section sufficient conditions that ensure asymptotic stability are developed and then discussed in the context of stability robustness. Letting $k \in [1, \ldots, N]$ and $l \in [1, \ldots, p]$, it is convenient to associate each of the $p \cdot N$ actuator laminas with unique indices $k$ and $l$. The $(k, l)$ piezolamina is then uniquely associated with a driving voltage $V_k^l(t)$, piezo-field function $\Lambda_k^l$, and piezo-property vector $(\boldsymbol{e}_0)_k^l$. Each of the dedicated $q \cdot N$ sensor laminas may be likewise assigned an indexed pair $(k, n)$ $(n \in [1, \ldots, q])$ and associated with $\Lambda_k^n$, $(\boldsymbol{e}_0)_k^n$ and a measured current $i_k^n(t)$ given by Eq. (8). If the $(k, l)$ layer is self-sensing, then the $(k, l)$ and $(k, n)$ piezolaminas are identical for some $n \in [1, \ldots, q]$. The following postulate is then introduced:

*Postulate 1:* Consider an anisotropic rectangular shell containing at least $p \cdot N$ piezolaminas whose equations of motion are given by Eq. (15). Then, if the entire set of control inputs $\{V_k^l(t)\}_{k=1,\ldots,N}^{l=1,\ldots,p}$ satisfy

$$\sum_{l=1}^{p}\sum_{k=1}^{N} V_k^l(t) \iint_A \frac{1}{A_1 A_2}(\mathcal{E}\boldsymbol{x}_t)^T (\boldsymbol{e}_0)_k^l \Lambda_k^l \,\mathrm{d}A \le 0 \tag{20}$$

the closed-loop system is asymptotically stable. If the $(k, l)$ piezolamina is self-sensing, then the closed-loop system is asymptotically stable if

$$\sum_{l=1}^{p}\sum_{k=1}^{N} V_k^l(t) i_k^l(t) \le 0 \tag{21}$$

*Proof:* Consider the following (positive definite) Lyapunov functional

$$J = \frac{1}{2}\iint_A \left[\rho h \boldsymbol{x}_t^T \boldsymbol{x}_t + \frac{1}{A_1 A_2}(\mathcal{E}\boldsymbol{x})^T \frac{1}{A_1 A_2}\begin{bmatrix} \boldsymbol{A} & \boldsymbol{B} \\ \boldsymbol{B} & \boldsymbol{D} \end{bmatrix}(\mathcal{E}\boldsymbol{x})\right]\mathrm{d}A \tag{22}$$

whose first and second terms in the integrand respectively represent the kinetic and mechanical strain energy states as derived in Ref. 9. The functional time derivative is then

$$\dot{J} = \iint_A \left[\rho h \boldsymbol{x}_t^T \boldsymbol{x}_{tt} + \frac{1}{A_1 A_2}(\mathcal{E}\boldsymbol{x}_t)^T \frac{1}{A_1 A_2}\begin{bmatrix} \boldsymbol{A} & \boldsymbol{B} \\ \boldsymbol{B} & \boldsymbol{D} \end{bmatrix}(\mathcal{E}\boldsymbol{x})\right]\mathrm{d}A \tag{23}$$

Integrating by parts and applying Eq. (3), Eq. (23) can be rendered into the form

$$\dot{J} = -\rho h \iint_A \boldsymbol{x}_t^T \mathcal{C}\boldsymbol{x}_t \,\mathrm{d}A + \sum_{l=1}^{p}\sum_{k=1}^{N} V_k^l \times \iint_A \frac{1}{A_1 A_2}(\mathcal{E}\boldsymbol{x}_t)^T (\boldsymbol{e}_0)_k^l \Lambda_k^l \,\mathrm{d}A \tag{24}$$

According to the second method of Lyapunov, the system is asymptotically stable if $\dot{J}$ is negative definite. Realize that Eq. (24) is synonymous with energy flux and that only the second term on the right-hand side (RHS) of the equation contains the influence of the piezoelectric layers. The first term represents the energy flux inherent to the passive system. Equation (6) establishes that the operator $\mathcal{C}$ is positive definite; hence, the first term is always dissipative, and the system will be asymptotically stable as long as the piezoelectrically induced forces do not add energy to the system. Asymptotic

stability is then contingent on the negative semidefiniteness of $\dot{J}_p$, where

$$\dot{J}_p \triangleq \sum_{l=1}^{p}\sum_{k=1}^{N} V_k^l \iint_A \frac{1}{A_1 A_2}(\mathcal{E}\boldsymbol{x}_t)^T (\boldsymbol{e}_0)_k^l \Lambda_k^l \, \mathrm{d}A \tag{25}$$

which is the condition stated in Eq. (20). Equation (21) then follows directly from Eq. (8). □

Postulate 1 can be used to establish a criterion for asymptotic stability, which is central to the development of stability robust SMC. Define $\boldsymbol{q}_a = [q_1 \cdots q_r]^T$ for use in the following theorem.

*Theorem 2:* Consider an anisotropic rectangular shell containing $p$ SMAs whose equations of motion are given by Eq. (19). Then if $\boldsymbol{V} = \boldsymbol{V}(\dot{\boldsymbol{q}}_a)$ is such that $\dot{\boldsymbol{q}}_a^T \boldsymbol{\alpha} \boldsymbol{V} \le 0$, the closed-loop system is asymptotically stable.

*Proof:* A required SMA construct condition is that $V_k^l(t) = (g_0)_k^l V_a^l(t)$ (Theorem 1). Hence, Eq. (25) becomes

$$\dot{J}_p \triangleq \sum_{l=1}^{p} V_a^l \sum_{k=1}^{N} \iint_A \frac{1}{A_1 A_2}(\mathcal{E}\boldsymbol{x}_t)^T (g_0)_k^l (\boldsymbol{e}_0)_k^l \Lambda_k^l \, \mathrm{d}A \tag{26}$$

Theorem 1 also establishes that

$$\sum_{k=1}^{N} \iint_A \frac{1}{A_1 A_2}(\mathcal{E}\boldsymbol{x}_t)^T (g_0)_k^l (\boldsymbol{e}_0)_k^l \Lambda_k^l \, \mathrm{d}A = \rho h \sum_{j=1}^{r} \alpha_j^l \lambda_j \dot{q}_j(t) \tag{27}$$

Substituting Eq. (27) into Eq. (26) and expressing the result in matrix form

$$\dot{J}_p = \rho h \left( \dot{\boldsymbol{q}}_a^T \boldsymbol{\alpha} \boldsymbol{V} \right) \tag{28}$$

the negative semidefiniteness of which is ensured by the condition stated in the theorem. □

Several corollaries of Theorem 2, whose proofs are readily established in Ref. 14, are critical to design SMC approaches that are stability robust. Denote the element by element Schur product[15] of two matrices $\boldsymbol{A}$ and $\boldsymbol{B}$ as $\boldsymbol{A} \circ \boldsymbol{B}$ and define $\mathrm{sgn}(\boldsymbol{i}) \triangleq [\mathrm{sgn}(i_s^1/\rho h) \cdots \mathrm{sgn}(i_s^q/\rho h)]^T$.

*Corollary 1:* Consider an anisotropic rectangular shell containing $p = q$ SSMAs such that $\boldsymbol{\alpha} = \boldsymbol{\beta}$ in Eq. (19). Then if $\boldsymbol{V} = -\boldsymbol{g}(t) \circ \mathrm{sgn}(\boldsymbol{i})$ for any arbitrary nonnegative function $\boldsymbol{g}(t) \in \Re^p$, the closed-loop system is asymptotically stable.

*Corollary 2:* Consider an anisotropic rectangular shell containing $p$ SMAs and $q$ SMSs whose equations of motion are given by Eq. (19). Let $\boldsymbol{V} = -\boldsymbol{G}(t)\boldsymbol{i}$ for any arbitrary $\boldsymbol{G} \in \Re^{p,q}$. Then if $\boldsymbol{\alpha}$ and $\boldsymbol{\beta}$ are such that $(\boldsymbol{\alpha}\boldsymbol{G}\boldsymbol{\beta}^T) \in \Re^{r,r}$ is positive semidefinite, the closed-loop system is asymptotically stable.

*Corollary 3:* Consider an anisotropic rectangular shell containing $p = q$ SSMAs such that $\boldsymbol{\alpha} = \boldsymbol{\beta}$ in Eq. (19). Let $\boldsymbol{V} = -\boldsymbol{G}(t)\boldsymbol{i}$ for any arbitrary $\boldsymbol{G} \in \Re^{p,p}$. Then if $\boldsymbol{G}$ is positive semidefinite, the closed-loop system is asymptotically stable.

*Corollary 4:* Consider an anisotropic rectangular shell containing $p$ SMAs and $q$ SMSs whose equations of motion are given by Eq. (19). Let $\min(p, q) = 1$ and let $\boldsymbol{V} = -\boldsymbol{G}(t)\boldsymbol{i}$ for any arbitrary $\boldsymbol{G} \in \Re^{p,q}$. Then if all elements of $\boldsymbol{\alpha}$, $\boldsymbol{\beta}$, and $\boldsymbol{G}$ are nonnegative, the closed-loop system is asymptotically stable.

Theorem 2 and its corollaries establish the five cases given in Table 1. Each case represents a set of constraints that can be imposed on the SMC objective to guarantee stability robustness. The generality of these constraints allows for stability robust designs to be realized without requiring the collocation of sensors and actuators (i.e., SSMAs). Although self-sensing actuation is advantageous from a theoretical standpoint, practical factors, such as frequency and temperature dependence of the external circuit,[12] may favor noncolocated transducers.

**Table 1 Stability criteria case study**

| Case | MPFs | $\mathrm{Min}(p, q)$ | Control law | Stability criterion |
|---|---|---|---|---|
| 1 | $\boldsymbol{\alpha} \ne \boldsymbol{\beta}$ | $\ge 1$ | $\boldsymbol{V} = \boldsymbol{V}(\dot{\boldsymbol{q}}_a)$ | $\dot{\boldsymbol{q}}_a^T \boldsymbol{\alpha} \boldsymbol{V} \le 0$ |
| 2 | $\boldsymbol{\alpha} = \boldsymbol{\beta}$ | $\ge 1$ | $\boldsymbol{V} = \boldsymbol{V}(\boldsymbol{i})$ | $\boldsymbol{V} = -\boldsymbol{g}(t) \circ \mathrm{sgn}(\boldsymbol{i})$ |
| 3 | $\boldsymbol{\alpha} \ne \boldsymbol{\beta}$ | $\ge 1$ | $\boldsymbol{V} = -\boldsymbol{G}\boldsymbol{i}$ | $\boldsymbol{\alpha}\boldsymbol{G}\boldsymbol{\beta}^T$ PSD |
| 4 | $\boldsymbol{\alpha} = \boldsymbol{\beta}$ | $\ge 1$ | $\boldsymbol{V} = -\boldsymbol{G}\boldsymbol{i}$ | $\boldsymbol{G}$ PSD |
| 5 | $\boldsymbol{\alpha} \ne \boldsymbol{\beta}$ | 1 | $\boldsymbol{V} = -\boldsymbol{G}\boldsymbol{i}$ | Elements $\boldsymbol{\alpha}, \boldsymbol{\beta}, \boldsymbol{G} \ge 0$ |

Case 1 is the most general of all cases listed, and it will be difficult to use the associated stability criterion to assess stability robustness. Case 2 is easily, but not necessarily, implemented via self-sensing actuation. When SSMAs are used, the requirement that $\boldsymbol{\alpha} = \boldsymbol{\beta}$ is ensured even when modeling and implementation errors yield actual MPFs that differ substantially from theoretical values. Case 3 is a general linear method in which stability robustness depends on the sensitivities of the eigenvalues of $\boldsymbol{\alpha}\boldsymbol{G}\boldsymbol{\beta}^T$ to perturbations in $\boldsymbol{\alpha}$ and $\boldsymbol{\beta}$. Case 4 is a linear subset of case 2. Case 5 provides a condition that can be verified through test: each targeted mode can be excited individually and the sign of each specific modal participation factor determined.

### C. Representative Performance Objectives

#### 1. Nonlinear Selective Energy Extraction

Several possible performance objectives are now explored. SMC approaches based on many other performance objectives can be found in Ref. 14. In the first example a nonlinear SMC method is derived (i.e., $\boldsymbol{\alpha}$, $\boldsymbol{\beta}$, and a control law are determined) whose objective is to explicitly define the contribution of each mode to the active energy extraction rate. Case 2 (Table 1) stability criteria are imposed so as to ensure a stability robust design; hence, $\boldsymbol{\alpha} = \boldsymbol{\beta}$, and the control law is $\boldsymbol{V} = -\boldsymbol{g}(t) \circ \mathrm{sgn}(\boldsymbol{i})$. Recalling that $\boldsymbol{i} = \boldsymbol{\alpha}^T \dot{\boldsymbol{q}}_a$ [via Eq. (17)], the control law becomes

$$\boldsymbol{V} = -\boldsymbol{g}(t) \circ \mathrm{sgn}(\boldsymbol{i}) = -\left[ g^1(t)\,\mathrm{sgn}\left(\sum_{j=1}^{r} \alpha_j^1 \lambda_j \dot{q}_j\right) \quad \cdots \quad g^p(t)\,\mathrm{sgn}\left(\sum_{j=1}^{r} \alpha_j^p \lambda_j \dot{q}_j\right)\right]^T \tag{29}$$

where $g^l(t)$ is the $l$th (PSD) element of $\boldsymbol{g}(t)$. Substituting Eq. (29) into Eq. (28), the energy flux can be expressed in the form

$$\dot{J}_p = -\rho h \sum_{l=1}^{p} g^l(t) \left| \sum_{j=1}^{r} \alpha_j^l \lambda_j \dot{q}_j(t) \right| \tag{30}$$

The character of the energy extraction rate can then be specifically determined by the arbitrarily chosen elements of $\boldsymbol{g}(t) \in \Re^p$. Two special cases are worth mentioning: if $p = 1$ and $\boldsymbol{g}(t) = 1$, then

$$\dot{J}_p = -\rho h \left| \sum_{j=1}^{r} \alpha_j \lambda_j \dot{q}_j(t) \right| \tag{31}$$

whereas if $p = r$, $\boldsymbol{g}(t) = [1 \quad \cdots \quad 1]^T$ and $\alpha_j^l = \alpha_j \delta_{jl}$, then

$$\dot{J}_p = -\rho h \sum_{j=1}^{r} |\alpha_j \lambda_j \dot{q}_j(t)| \tag{32}$$

From a structural point of view, Eq. (31) is the simplest possible case (only a single SMT is required), whereas Eq. (32) is the most complex (one SMT per mode). Nonetheless Eq. (32), unlike Eq. (31), avoids the existence of nontrivial state trajectories for which $\dot{J}_p = 0$ and hence guarantees active energy extraction along any trajectory.

#### 2. Linear Selective Energy Extraction

When the case 3 (Table 1) scenario is obeyed so that the control law is $\boldsymbol{V} = -\boldsymbol{G}\boldsymbol{i}$, then the energy flux expression [Eq. (28)] becomes

$$\dot{J}_p = -\rho h \left[ \dot{\boldsymbol{q}}_a^T (\boldsymbol{\alpha}\boldsymbol{G}\boldsymbol{\beta}) \dot{\boldsymbol{q}}_a \right] \tag{33}$$

from which an energy-based linear method can be derived. The performance objective is to select $\boldsymbol{\alpha}$, $\boldsymbol{\beta}$, and $\boldsymbol{G}(t)$ so as to maximize the energy extracted from each targeted mode relative to a specified

weighting. The control law transforms Eq. (19) into the (closed-loop) system equation

$$\dot{\boldsymbol{x}}_a = \boldsymbol{A}_a \boldsymbol{x}_a, \qquad \boldsymbol{A}_a \triangleq \boldsymbol{A} - \begin{bmatrix} 0 & 0 \\ 0 & \boldsymbol{\alpha G \beta}^T \end{bmatrix} \tag{34}$$

Integrating Eq. (33) over the time interval $t = [0, t_f]$, the total energy that is actively added to the system via the piezoelectric laminas is then

$$J_p = -\rho h \int_0^{t_f} \left[ \dot{\boldsymbol{q}}_a^T (\boldsymbol{\alpha G \beta}) \dot{\boldsymbol{q}}_a \right] \mathrm{d}t \tag{35}$$

Introducing an arbitrarily specified state weighting matrix $\bar{\boldsymbol{Q}} \in \Re^{r,r}$, an optimal gain matrix $\boldsymbol{G}(t)$ and set of MPFs (contained in $\boldsymbol{\alpha}, \boldsymbol{\beta}$) can be determined through the maximization of the performance index

$$\mathcal{J} = \int_0^{t_f} \left[ \boldsymbol{x}_a^T \ \boldsymbol{Q} \boldsymbol{x}_a \right] \mathrm{d}t, \qquad \boldsymbol{Q} \triangleq \begin{bmatrix} 0 & 0 \\ 0 & \bar{\boldsymbol{Q}}^T \boldsymbol{\alpha G \beta} \bar{\boldsymbol{Q}} \end{bmatrix} \tag{36}$$

subject to Eq. (34). Because the optimal solution is stable, $\boldsymbol{\alpha G \beta}$ is PSD, and stability robustness is assessed through sensitivity of its eigenvalues to perturbations in $\boldsymbol{\alpha}$ and $\boldsymbol{\beta}$. If $\boldsymbol{\alpha} = \boldsymbol{\beta}$ (case 4, Table 1), then stability robustness is ensured a priori. However, enforcing that $\boldsymbol{\alpha} = \boldsymbol{\beta}$ will inevitably lead to an optimal value of the performance index that will be less than the value obtained via the case 3 optimization (hence less effective control) because fewer parameters are allowed in the optimization.

*3. Eigenvalue Selection*

Again returning to the general linear (case 3, Table 1) scenario, the performance objective now considered is to find $\boldsymbol{\alpha}$, $\boldsymbol{\beta}$, and $\boldsymbol{G}$ so as to move the open-loop poles as close as possible to a specified set of desired locations. Defining

$$\boldsymbol{p}(\boldsymbol{A}_a) \triangleq [p_1 \quad \cdots \quad p_{2r}]^T \tag{37}$$

$$\boldsymbol{p}_0 \triangleq [(p_1)_0 \quad \cdots \quad (p_{2r})_0]^T \tag{38}$$

where $p_j$ is the $j$th (possibly complex) pole location of $\boldsymbol{A}_a$ and $(p_j)_0$ is the desired $j$th pole location, then the performance objective can be realized through the minimization of

$$\mathcal{J} = (\boldsymbol{p} - \boldsymbol{p}_0)^T \boldsymbol{Q} (\boldsymbol{p} - \boldsymbol{p}_0) \tag{39}$$

subject to Eq. (34), where $\boldsymbol{Q} \in \Re^{2r,2r}$ is a PSD symmetric weighting matrix.

## V. Numerical Example

A numerical example is now given, which serves to both illustrate the SMC design process and to verify the analytical results already developed. A general design procedure is identified and then implemented in order to arrive at an SMC design for a anisotropic cantilevered cylindrical semisection in which the damping factors of the first three modes are chosen optimally. A parameter optimization process is used to derive a suitable set of MPFs and a control law. Implementation is realized via a single SSMA. The SMC design is then validated through numerical simulation.

*Step 1 Structural Design:* The first step in the design process is to determine the structural design of the composite shell so as to satisfy any mechanical requirements. A cantilevered cylindrical panel is considered, whose geometry is given in Fig. 2. The panel itself is, in essence, a semisection that spans 60 deg of a cylinder with a fixed radius $R$ such that the ($\alpha_2$ dimension) width is 0.4 m. The section length is 0.6 m. Three mechanically isotropic and piezoelectrically biaxial PVDF layers are bonded to each surface of a double-layered graphite-epoxy composite substrate, and the layers are sequentially numbered from top to bottom. Relevant material properties are given in Tables 2 and 3.

*Step 2 Model Generation:* Using the ANSYS finite element modeling (FEM) package,[16] a discrete model of the passive system was developed based on a 169-node finite element representation of the cylindrical panel. Mass, damping, and stiffness matrices were thus obtained. The first three mode shapes are shown in Fig. 3 (curvilinear coordinates). The first ten open-loop natural frequencies and damping ratios are listed in Table 4.

*Step 3 Performance Objective:* The structure is excited initially through a disturbance force $d(t)$ acting at a free corner, as shown in Fig. 2. In this example problem the performance objective is to increase damping in the first three modes via maximization of the objective functional $J = \min(\zeta_j \omega_j)$, for $j = (1, 2, 3)$. Expressing the reduced system in the form of Eq. (34) (where $\boldsymbol{A} \in \Re^{6,6}$) and

**Table 2 Material properties for example structure**

| Property | PVDF | G-epoxy |
|---|---|---|
| $E_{11}$, Pa | $2.00 \times 10^9$ | $14.5 \times 10^9$ |
| $E_{22}$, Pa | $2.00 \times 10^9$ | $9.60 \times 10^9$ |
| $G_{12}$, Pa | $1.42 \times 10^9$ | $4.10 \times 10^9$ |
| $\nu_{12}$ | 0.3 | 0.3 |
| $\rho$, kg/m$^3$ | 1780 | 1551 |
| $(e_{31}^0)_{\theta=0^\circ}$, Coul/m$^2$ | $60 \times 10^3$ | —— |
| $(e_{32}^0)_{\theta=0^\circ}$, Coul/m$^2$ | $20 \times 10^3$ | —— |

**Table 3 Sublaminas skew angles and thicknesses**

| | PVDF (top) | | | G-epoxy (middle) | | PVDF (bottom) | | |
|---|---|---|---|---|---|---|---|---|
| Layer | 1 | 2 | 3 | 4 | 5 | 6 | 7 | 8 |
| Skew angle, deg | 60 | 0 | −60 | 45 | −45 | −60 | 0 | 60 |
| Thickness, $\mu$m | 28 | 28 | 28 | 140 | 140 | 28 | 28 | 28 |

**Table 4 Passive and active system damping coefficients and natural frequencies**

| | Open loop | | Ideal closed loop | | Actual closed loop | |
|---|---|---|---|---|---|---|
| Mode | $\zeta_m$ | $\omega_m$, rad/s | $\zeta_m$ | $\omega_m$, rad/s | $\zeta_m$ | $\omega_m$, rad/s |
| 1 | 0.00748 | 29.93 | 0.40848 | 39.13 | 0.40215 | 39.14 |
| 2 | 0.01473 | 58.91 | 0.29581 | 51.20 | 0.29264 | 50.67 |
| 3 | 0.03583 | 143.3 | 0.29315 | 126.1 | 0.28973 | 127.3 |
| 4 | 0.03594 | 145.8 | 0.03594 | 145.8 | 0.03653 | 146.2 |
| 5 | 0.03898 | 155.9 | 0.03898 | 155.9 | 0.03821 | 156.9 |
| 6 | 0.04395 | 175.8 | 0.04395 | 175.8 | 0.04474 | 173.7 |
| 7 | 0.06420 | 256.8 | 0.06420 | 256.8 | 0.06310 | 255.3 |
| 8 | 0.06437 | 261.5 | 0.06437 | 261.5 | 0.06458 | 259.7 |
| 9 | 0.06836 | 273.4 | 0.06836 | 273.4 | 0.06953 | 274.8 |
| 10 | 0.08987 | 359.5 | 0.08987 | 359.5 | 0.09126 | 363.5 |

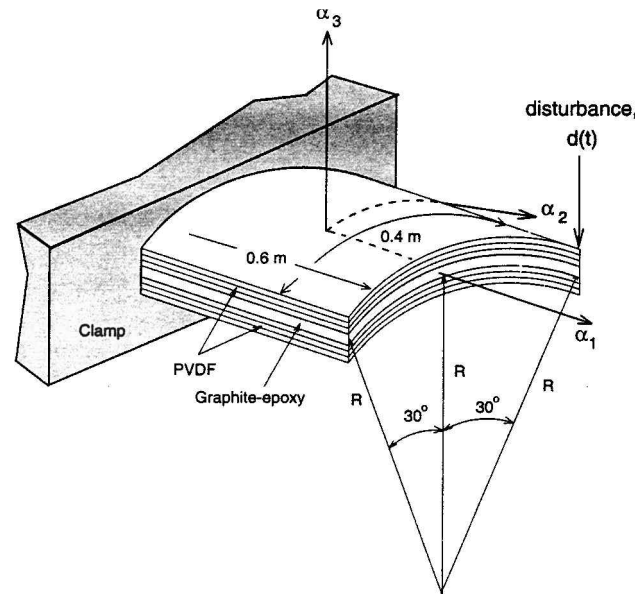


**Fig. 2 Cylindrical panel example problem geometry.**

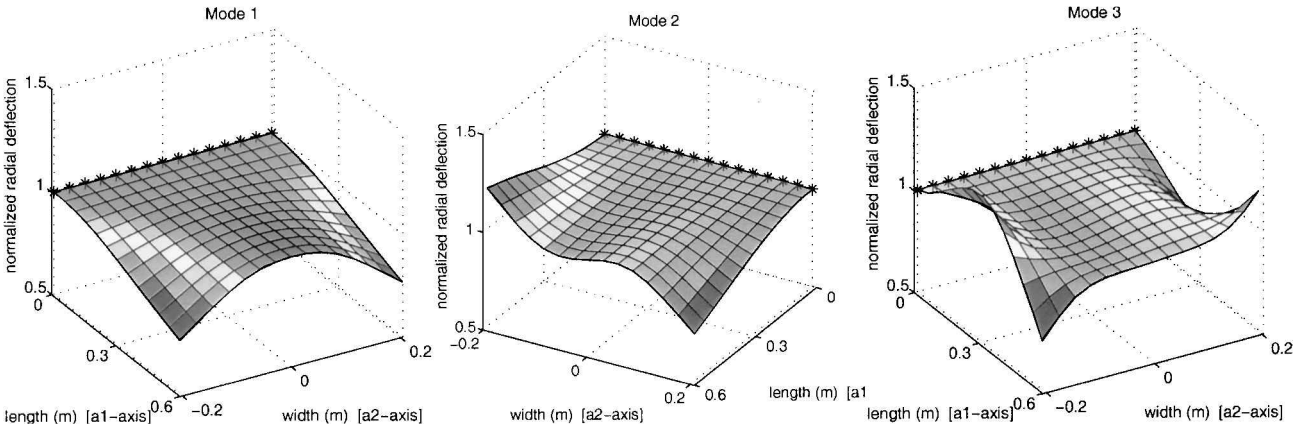


**Fig. 3 First three structural mode shapes in curvilinear coordinate frame (deflections are scaled). Starred boundary indicates a clamped condition.**

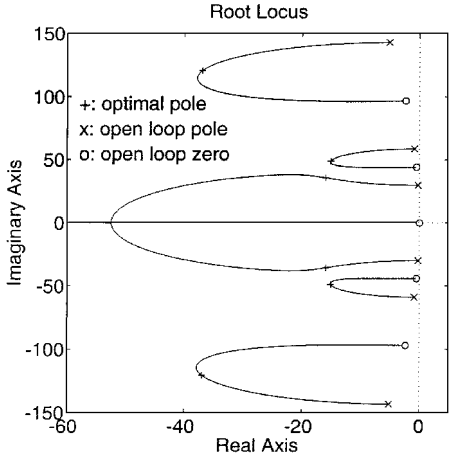


**Fig. 4 System root locus for different values of $G$ using optimal MPF values.**

maximizing $J$ with respect to the MPFs via a (self-written) steepest ascent algorithm, the optimal values

$$(\alpha_1, \alpha_2, \alpha_3, G) = (0.002971, 0.000825, 0.0002415, 3.102)$$

were obtained. Figure 4 describes how the pole locations of the open-loop system [Eq. (19)] are moved in the complex plane when the optimal MPF values are assumed and the feedback gain $G$ is allowed to vary. The closed-loop pole locations at the optimal gain value are marked in the figure with a plus (+) sign. Open- and closed-loop damping coefficients and natural frequencies, which are determined directly from the obtained (complex) pole locations, are listed in Table 4 as the ideal values. Note that it was unnecessary to bound the control input through the introduction of a control-related term in the performance index (i.e., add to the objective functional a term of the form $\int_0^\infty r_0 V_a^2 \, \mathrm{d}t$, where $r_0 > 0$) because the closed-loop poles naturally migrate to the nonoptimal locations of the open-loop zeros as the control gain is increased to infinity.

*Step 4 Piezo-Field Functions:* Having determined the targeted subsystem mode shapes and MPFs, the piezoelectric field functions are then determined via Eq. (11). Based on the optimal MPF values and data given in Tables 2 and 3, field function descriptions for each of the six active layers are then determined via numerically approximating Eq. (11) and are shown in Fig. 5. The corresponding set of scaling factors, $g_0^k$ for layers 1–6 were found to be 14.92, 6.36, 8.13, 12.31, 7.07, and 9.10, respectively.

Having completed the design process, the SSMA design and SMC control law would normally be implemented on the actual structure. For the sake of verifying both the SMT theory and the SMC results, actual structural implementation is replaced here with a numerical simulation. For convenience

$$\mathcal{C} = b_0 \mathcal{I} + c_0 \mathcal{K} \tag{40}$$

which is one of many choices that would satisfy Eq. (6) ($\mathcal{I}$ is the identity operator). Premultiplying the equation of motion [Eq. (3)] by $\rho h A_1 A_2$ and recalling that $V^k(t) = g_0^k V_a(t)$ such that

$$\rho h A_1 A_2 \boldsymbol{x}_{tt} + \rho h A_1 A_2 \mathcal{C} \boldsymbol{x}_t + \rho h A_1 A_2 \mathcal{K} \boldsymbol{x} = -\left[ \mathcal{D}^T \left( \sum_{k=1}^{N} g_0^k \boldsymbol{e}_0^k \Lambda^k \right) \right] V_a \tag{41}$$

the FEM model (step 1) was derived by ignoring the RHS and discretizing the left-hand side of Eq. (41) so as to arrive at a numerical model in the form

$$M\ddot{\boldsymbol{x}} + C\dot{\boldsymbol{x}} + K\boldsymbol{x} = 0 \tag{42}$$

where $\boldsymbol{x}$ is a time-dependent vector of $\alpha_1, \alpha_2, \alpha_3$ displacements at each node location. Using the piezo-field functions just determined and including the disturbance force $d(t)$, the state equations are augmented through the discretization of the RHS of Eq. (41):

$$M\ddot{\boldsymbol{x}} + C\dot{\boldsymbol{x}} + K\boldsymbol{x} = \boldsymbol{f} V_a + \boldsymbol{d}\, d(t) \tag{43}$$

where $\boldsymbol{d}$ is a unit vector whose only nonzero element corresponds to the $\alpha_3$ translation of the single node at which the disturbance is applied (Fig. 2). Then limiting the amount of modes of interest to 20 for the purpose of simulation, a modal transformation of the form $\boldsymbol{x} = \boldsymbol{V}\boldsymbol{q}$ was performed on Eq. (43), where $\boldsymbol{V}$ is a matrix whose columns are the first 20 eigenvectors of Eq. (43) and $\boldsymbol{q}$ is a 20-element column vector containing the first 20 modal coordinates. The modal system representation is then given as

$$\ddot{\boldsymbol{q}} + \bar{\boldsymbol{C}}\dot{\boldsymbol{q}} + \bar{\boldsymbol{K}}\boldsymbol{q} = \boldsymbol{f}_q V_a(t) + \boldsymbol{d}_q\, d(t) \tag{44}$$

where $\bar{\boldsymbol{C}}$ and $\bar{\boldsymbol{K}}$ are diagonal matrices whose respective elements contain the terms $b_0 + c_0\lambda_m$ and $\lambda_m$. The elements of $\boldsymbol{f}_q$ were observed to be very nearly equal to $\alpha_m \lambda_m$, although numerical differentiation gave rise to marginal errors. In particular the closed-loop damping and natural frequency data that were obtained through Eq. (44) are listed as the actual values in Table 4. The actual values compare favorably with the listed ideal values, which are those values that assumedly would have been obtained if there were no numerical errors. Note that modes 7–10, which are outside the targeted modal subset, are virtually not influenced through active control because the SMTs function as predicted.

To facilitate a performance analysis, a reference measurement $m(t)$ is added whose output is the $\alpha_3$ displacement of the panel at the point at which the disturbance is applied. Hence, upon conversion of Eq. (44) to the form of Eq. (19), the augmented system equations are

$$\frac{\mathrm{d}}{\mathrm{d}t}\begin{bmatrix} \boldsymbol{q} \\ \dot{\boldsymbol{q}} \end{bmatrix} = \begin{bmatrix} 0 & 1 \\ -\bar{\boldsymbol{K}} & -\bar{\boldsymbol{C}} \end{bmatrix}\begin{bmatrix} \boldsymbol{q} \\ \dot{\boldsymbol{q}} \end{bmatrix} + \begin{bmatrix} 0 \\ \boldsymbol{f}_q \end{bmatrix} V_a + \begin{bmatrix} 0 \\ \boldsymbol{d}_q \end{bmatrix} d \tag{45}$$

$$\begin{bmatrix} i \\ m \end{bmatrix} = \begin{bmatrix} 0 & \boldsymbol{f}_q^T \\ \boldsymbol{d}_q^T & 0 \end{bmatrix}\begin{bmatrix} \boldsymbol{q} \\ \dot{\boldsymbol{q}} \end{bmatrix} \tag{46}$$

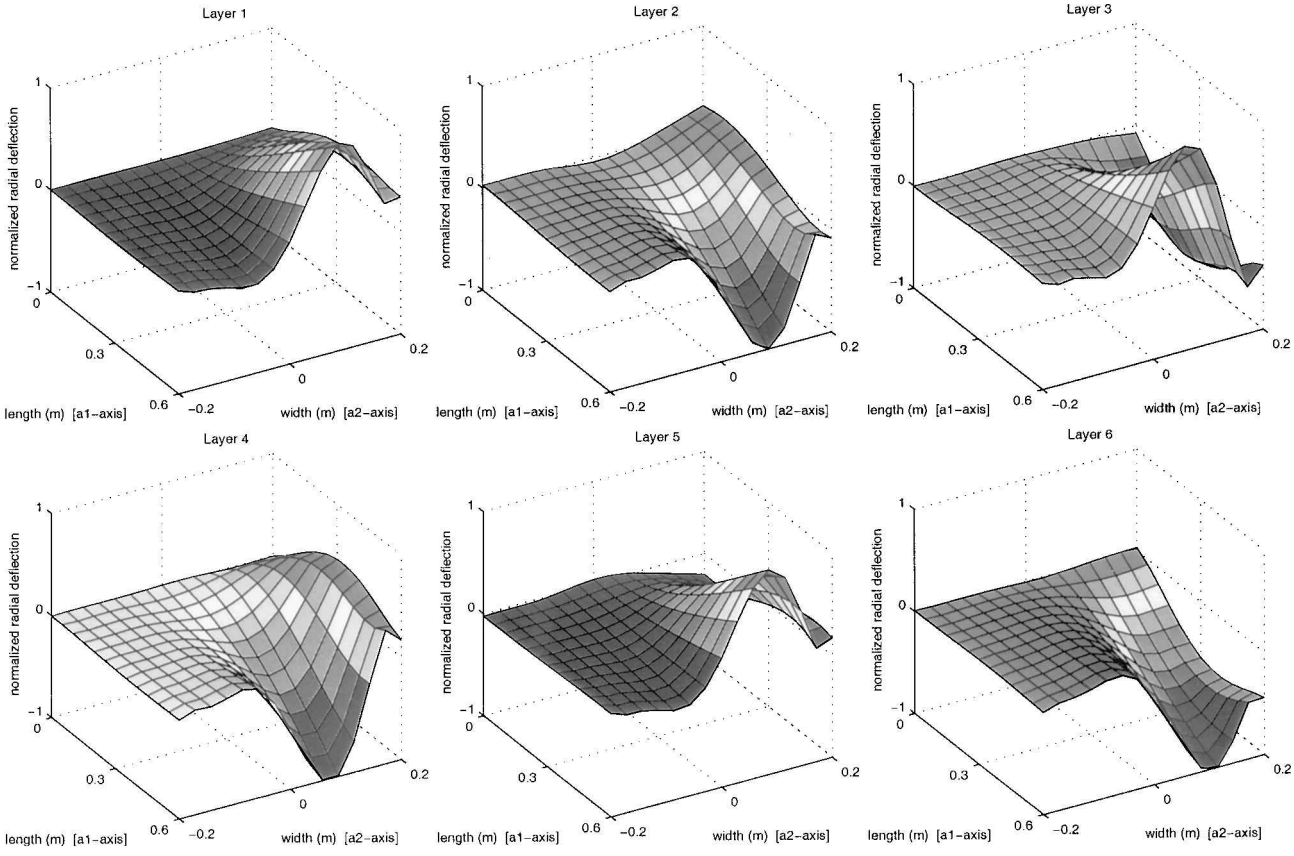


**Fig. 5 Piezo-field functions for the SSMA sublaminas 4–6, relative to the curvilinear coordinate frame.**

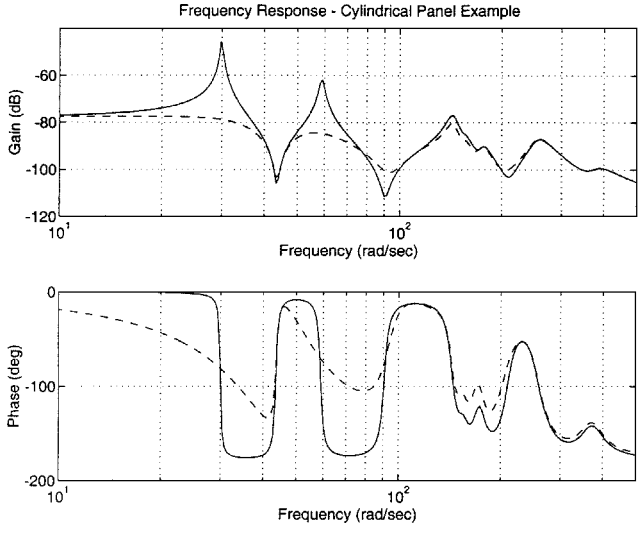


**Fig. 6 Frequency response of $m(s)/d(s)$. Solid and dashed lines respectively indicate open- and closed-loop response.**

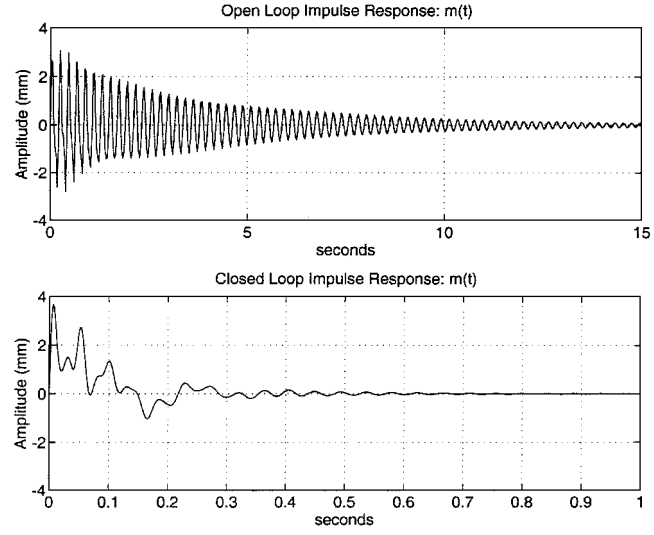


**Fig. 7 System response to an impulse disturbance $d(t)$.**

where $i(t) \triangleq (1/\rho h) i_s(t)$. The required feedback law is then

$$V_a = [-G \quad 0] \begin{bmatrix} i \\ m \end{bmatrix} \tag{47}$$

Open- and closed-loop frequency and transient response analyses were computed using the preceding system description. Closed-loop damping factors and natural frequencies are listed in Table 4 as the actual values and compare well to the ideal values determined directly through the optimization procedure. The Bode magnitude and phase plots of the transfer function $m(s)/d(s)$ are given in Fig. 6. Solid lines refer to the passive system response while dashed lines indicate the active system response. Figure 6 shows substantial closed-loop attenuation of the first three modes while all higher-order modes remain essentially unaffected. In computing the transient response given in Fig. 7, a unit impulse disturbance was applied through $d(t)$, and the transient response as measured through the reference measurement $m(t)$ was recorded. The closed-loop settling time is substantially more rapid. The results validate the SMC design approach as applied to curvilinear anisotropic structures.

## VI. Conclusions

A general design procedure for the realization of SMC has been presented for piezolaminated anisotropic shell systems. General stability criteria were established from which stability robust SMC approaches can be derived. Sensor-actuator collocation is not required. Several representative objective functions were given. Many

stability robust SMC implementations were shown to be realizable with only a single SMT and proportional feedback. The SMC design procedure was demonstrated through a numerical example involving a composite piezolaminated anisotropic cylindrical panel. The outcome of that procedure, a unique transducer design and accompanying control law derived through the parameter optimization of a specified objective function, was then validated through numerical simulation. Transient and frequency response analyses demonstrate a significant improvement in system performance via the SMC approach relative to conventional methods.

Although a theory and design approach was established for using a small set of active piezolaminas in an anisotropic composite as a basis for modal control, this paper did not attempt to explore the practical implementation aspects of this technique. In an experimental implementation of the method on an orthotropic plate,[8] the authors identified factors, such as bonding and electromagnetic interference, that should be considered by the industry. Although the approach effectively harnesses the limited transduction authority of polyvinyledine fluoride piezo-transducers through an optimization process, the presented theory will be equally applicable to more advanced transducers as they become available.

## References

[1]Bailey, T., and Hubbard, J., "Distributed Piezoelectric Polymer Active Vibration Control of a Cantilever Beam," *Journal of Guidance, Control, and Dynamics*, Vol. 8, No. 5, 1985, pp. 605–611.

[2]Burke, S., and Hubbard, J. E., "Distributed Actuator Control Design for Flexible Beams," *Automatica*, Vol. 24, No. 5, 1988, pp. 619–627.

[3]Miller, S. E., and Hubbard, J. E., "Smart Components for Structural Vibration Control," *Proceedings of the 1988 American Controls Conference*, Vol. 3, Inst. of Electrical and Electronics Engineers, New York, 1988, pp. 1897–1902.

[4]Burke, S. E., and Hubbard, J. E., "Distributed Transducer Control Design for Thin Plates," *Proceedings of the Conference on Electro-Optical Materials for Switches, Coatings, Sensor Optics, and Detectors*, Vol. 1307, Society of Photo-Optical Instrumentation Engineers, Bellingham, WA, 1990, pp. 222–231.

[5]Lee, C. K., "Theory of Laminated Piezoelectric Plates for the Design of Distributed Sensors and Actuators. Part 1: Governing Equations and Reciprocal Relationships," *Journal of the Acoustical Society of America*, Vol. 87, No. 3, 1990, pp. 1144–1158.

[6]Miller, S., Abramovich, H., and Oshman, Y., "Active Distributed Vibration Control of Anisotropic Piezoelectric Laminated Plates," *Journal of Sound and Vibration*, Vol. 183, No. 5, 1995, pp. 797–817.

[7]Miller, S. E., Oshman, Y., and Abramovich, H., "Modal Control of Piezolaminated Anisotropic Rectangular Plates. Part 2: Control Theory," *AIAA Journal*, Vol. 34, No. 9, 1996, pp. 1876–1884.

[8]Miller, S. E., Abramovich, H., and Oshman, Y., "Experimental Validation of a Modal Transducer for an Orthotropic Rectangular Plate," *AIAA Journal*, Vol. 35, No. 10, 1997, pp. 1621–1629.

[9]Reddy, J. N., *Energy and Variational Methods in Applied Mechanics*, Wiley, New York, 1984, pp. 183–195.

[10]Soedel, W., *Vibrations of Shells and Plates*, Marcel Dekker, New York, 1981, pp. 229–235.

[11]Miller, S. E., Oshman, Y., and Abramovich, H., "Selective Modal Transducers for Piezolaminated Anisotropic Shells," *Journal of Guidance, Control, and Dynamics*, Vol. 22, No. 3, 1999, pp. 455–466.

[12]Dosch, J., Mayne, R., and Inman, D., "Dual Function System Having a Piezoelectric Element," U.S. Patent No. 5347870, Sept. 1994.

[13]Meirovitch, L., *Dynamics and Control of Structures*, Wiley, New York, 1990, pp. 180–182.

[14]Miller, S. E., "Distributed Modal Control of Piezolaminated Anisotropic Planar and Cylindrical Structures," Ph.D. Dissertation, Faculty of Aerospace Engineering, Technion—Israel Inst. of Technology, Haifa, Israel, Sept. 1995.

[15]Horn, R. A., and Johnson, C. A., *Matrix Analysis*, Cambridge Univ. Press, Cambridge, England, U.K., 1985, p. 455.

[16]Swanson Analysis Systems, *ANSYS User's Manual for Revision 5.0*, Canonsburg, PA, 1992.